



**HAL**  
open science

## Synthesis of a Se<sub>0</sub>/Calcite Composite Using Hydrothermal Carbonation of Ca(OH)<sub>2</sub> Coupled to a Complex Selenocystine Fragmentation

G. Montes-Hernandez, L. Charlet, F. Renard, A. C. Scheinost, Maïté Bueno, A. Fernandez Martinez

► **To cite this version:**

G. Montes-Hernandez, L. Charlet, F. Renard, A. C. Scheinost, Maïté Bueno, et al.. Synthesis of a Se<sub>0</sub>/Calcite Composite Using Hydrothermal Carbonation of Ca(OH)<sub>2</sub> Coupled to a Complex Selenocystine Fragmentation. *Crystal Growth & Design*, 2008, 8 (7), pp.2497 à 2504. 10.1021/cg800141p . insu-00351971

**HAL Id: insu-00351971**

**<https://insu.hal.science/insu-00351971>**

Submitted on 12 Jan 2009

**HAL** is a multi-disciplinary open access archive for the deposit and dissemination of scientific research documents, whether they are published or not. The documents may come from teaching and research institutions in France or abroad, or from public or private research centers.

L'archive ouverte pluridisciplinaire **HAL**, est destinée au dépôt et à la diffusion de documents scientifiques de niveau recherche, publiés ou non, émanant des établissements d'enseignement et de recherche français ou étrangers, des laboratoires publics ou privés.



1 **Abstract**

2

3 In this study, the hydrothermal carbonation of calcium hydroxide under high CO<sub>2</sub>-Ar pressure  
4 (90 bar) and high temperature (90 °C) coupled with a complex selenocystine fragmentation  
5 was carried out by using a batch system in order to synthesize an elemental selenium  
6 (Se<sup>0</sup>)/calcite composite. Under O<sub>2</sub>-poor conditions, the composite was mainly characterized  
7 by red spherical selenium nanoparticles “non crystalline elemental selenium” (<500nm)  
8 deposited on the calcite matrix. In contrast, under O<sub>2</sub>-rich conditions, the composite was  
9 characterized by grey rods selenium microparticles “crystalline elemental selenium” (<25µm)  
10 dispersed in the calcite matrix. The carbonate matrix was constituted by nano- and micro-  
11 rhombohedral crystals (<2µm) and micrometric agglomerates and/or aggregates (<5µm).  
12 The results presented here demonstrate that Se<sup>0</sup>/calcite composite, with spherical or rod  
13 morphologies for elemental selenium can be produced, this composite could possibly has a  
14 high potential for medical (ex. dietary supplement) or industrial (ex. pigments) applications.  
15 In addition, this study may have implications in the field of biomineralization.

16

17

18 **Keywords:** Elemental selenium, Calcite, Composite, Growth, Selenocystine,  
19 Nanoparticles, Hydrothermal method

20

21

22

23

24

25

## 1 **1. Introduction**

2

3 Selenium is well known for its photochemical and semiconductor properties and has been  
4 successfully used in solar cells, rectifiers, photographic exposure meters and xerography [1-  
5 3]. Selenium is also a key trace element required in small quantities in humans and animals  
6 for the function of a number of selenium-dependent enzymes, such as glutathione peroxidase  
7 (GPX) and thioredoxin reductase; however this element can also be toxic in larger doses.  
8 Both the beneficial and toxic effects of selenium are based on concentration ingested and on  
9 its chemical forms [4-10]. Inorganic and organic forms have been identified in the Nature. In  
10 addition, the selenium can easily form compounds with metals and occurs in about 50  
11 minerals. It is present in four different oxidation states in aqueous and subsurface systems,  
12 namely -2, 0, +4 and +6 [11-13]. Obviously, the fate and transport of Se in contaminated sites  
13 are very much influenced by its chemical form and speciation.

14 Recently, elemental selenium nanoparticles have been fabricated through various approaches,  
15 such us laser ablation, solution-phase approach, vapour-phase growth, electrochemical  
16 synthesis, photothermally assisted solution phase, ultrasonic, hydrothermal or solvothermal  
17 method and micelle-mediated synthesis [1]. Searching and designing novel methods to  
18 synthesize elemental selenium with controlled morphology is important from the viewpoint of  
19 fundamental issues and application. For example, recently, the  $\text{Se}^0$  nanoparticles are attracting  
20 more and more attention due to their excellent high biological activity and lower toxicity in  
21 animals and man.

22 Calcium carbonate is an inorganic compound that has been widely studied due to its  
23 abundance in nature as a mineral and biomineral. Calcium carbonate particles are found in  
24 three polymorph structures, which are generally classified as rhombic calcite, needle-like  
25 aragonite and spherical vaterite. Calcite belonging to Trigonal-Hexagonal-Scaleno-hedral

1 crystallographic class is the most stable phase at room temperature under normal atmospheric  
2 conditions, while aragonite and vaterite belong to Orthorombic-Dipyramidal class and  
3 Hexagonal-Dihexagonal Dipyramidal class, respectively. The later are metastable polymorphs  
4 which readily transform into the stable calcite. The specific formation of one of the  
5 polymorphs of crystalline calcium carbonate particles depends mainly on the precipitation  
6 conditions, such as pH, temperature and supersaturation. Supersaturation is usually  
7 considered to be the main controlling factor [14]. Many experimental studies have been  
8 reported about the synthetic precipitation of the various forms of calcium carbonate and the  
9 conditions under which these may be produced, including the importance of initial  
10 supersaturation, temperature, pressure, pH and hydrodynamics. The effect of impurities and  
11 additives has also been well studied [15-29].

12 The above short description shows that the formation of calcite ( $\text{CaCO}_3$ ) and elemental  
13 selenium ( $\text{Se}^0$ ) are complex processes of considerable importance and numerous studies have  
14 been reported in the literature. The co-existence and the simultaneous precipitation/growth of  
15 these solid structures, however, have not been studied and/or reported to our knowledge. In  
16 this study, the hydrothermal carbonation of calcium hydroxide under high  $\text{CO}_2$ -Ar pressure  
17 (90 bar) coupled with a complex selenocystine fragmentation under  $\text{O}_2$ -poor and  $\text{O}_2$ -rich  
18 conditions was carried out by using a semi-batch system (sampling with time) in order to  
19 synthesize an elemental selenium ( $\text{Se}^0$ )/calcite composite.

20 Several analytical techniques were performed in order to characterize selected solid samples  
21 (SEM/EDS, TEM/EDS, XRD and XANES and EXAFS spectroscopy) and selected solution  
22 samples (ICP/AES and HPLC/ICPMS).

23

24

25

## 2. Materials and methods

### 2.1. Synthesis of $Se^0$ /calcite composite

(a) Under  $O_2$ -poor conditions or system with a purge step

One litre of high-purity water with electrical resistivity of  $18.2 \text{ M}\Omega\cdot\text{cm}$ , 3 g of commercial portlandite  $\text{Ca}(\text{OH})_2$  (calcium hydroxide provided by Sigma-Aldrich) with 96% chemical purity (3%  $\text{CaCO}_3$  and 1% other impurities) and different quantities (0, 50, 100 or 200 mg) of seleno-L-cystine  $\text{CO}_2\text{HCH}(\text{NH}_2)\text{CH}_2(\text{Se})_2\text{CH}_2\text{CH}(\text{NH}_2)\text{CO}_2\text{H}$  (provided by Sigma-Aldrich) with chemical purity ( $\geq 98.0\%$ ) were placed in a titanium reactor (Parr© autoclave with internal volume of two litres). The hydroxide and selenocystine particles were immediately dispersed with mechanical agitation (400 rpm). Then, at room temperature the gas argon with 99.999% chemical purity (provided by Linde Gas S.A.) was injected into the reaction cell in order to control the pressure at 90 bar during 30 minutes. After this time period, the suspension was heated to  $90^\circ\text{C}$  with a furnace adapted to the reactor. Obviously, during heating stage the pressure increased into the system, but it was kept constant at about 90 bar by using successive manual purge until the temperature was stabilized (about 90 minutes). Then, about 20 ml of suspension were sampled in the reactor ( $t=0$ ) and immediately a flash purge was carried out until atmospheric pressure was reached. Theoretically, the argon adsorption in the suspension, the heating stage and the gas purge, allowed a partial removal of dissolved oxygen from the suspension ( $O_2$ -poor conditions). Unfortunately, the oxygen concentration was not monitored into the reaction cell. When the atmospheric pressure was reached in the reactor, 14.5 g of  $\text{CO}_2$  with 99.995% chemical purity (provided by Linde Gas S.A.) were injected in the reactor and the total pressure in the system was immediately adjusted to 90 bar by argon injection. Under these T and P conditions, the vapour phase consists mainly of an  $\text{Ar}+\text{CO}_2$  mixture with the  $\text{CO}_2$  in a supercritical state (see Figure 1).

1 After this, a semi-batch system (sampling with time) was performed in order to measure the  
2 pH (using MA235 pH/ion analyzer) and, calcium and selenium concentration (using ICP  
3 Perkin Elmer Optima 3300 DV) in filtered solutions. For this case, about 20 ml of suspension  
4 were sampled in the reactor as a function of time ( $t=2, 6, 10, 30$  and 60 minutes) during  
5 composite formation. Note that the pH measurement was carried out at 25 °C after filtration,  
6 cooling and degasification of the solutions. Obviously, this measurement is not representative  
7 of in situ pH behaviour, but, it can give a reasonable quantification of the solution saturation  
8 index with respect to the solid phases at standard conditions (25 °C and 1 atmosphere).

9 At the end of the experiment, the autoclave was removed from the heating system and  
10 immersed in cold water. The reaction cell was depressurized during the water cooling period.  
11 After water cooling at 35°C (about 15 minutes) the autoclave was disassembled, and the solid  
12 product was carefully recovered and separated by centrifugation (30 minutes at 12,000 rpm),  
13 decanting the supernatant solutions. Finally, the solid product was dried directly in the  
14 centrifugation flasks for 72 h at 65°C, manually recovered and stocked in plastic flasks.

15

16 (b) Under O<sub>2</sub>-rich conditions or system without a purge step

17 For these experiments, the dispersions (water-calcium hydroxide-selenocystine) cited above  
18 were directly heated to 90°C at atmospheric pressure. When the temperature was stabilized,  
19 about 20 ml of suspension were sampled in the reactor ( $t=0$ ). Then, 14.5 g of CO<sub>2</sub> were  
20 injected into the reactor and the total pressure in the system was immediately adjusted at 90  
21 bar by argon injection. After the pressure setting, the sampling and composite recovery  
22 procedures were identical to the O<sub>2</sub>-poor system described above.

23 Height different experiments were carried out, four under O<sub>2</sub>-poor conditions and four under  
24 O<sub>2</sub>-rich conditions. For each experiment, six suspension samples were withdrawn from the

1 reactor. In addition, the experiments with 200 mg of selenocystine under O<sub>2</sub>-poor and O<sub>2</sub>-rich  
2 conditions were repeated three times in order to check their colour reproducibility.

3

## 4 *2.2. Composite characterization*

### 5 (a) Macroscopic observations

6 The coloration change with reaction time was registered by using a simple charge-coupled  
7 device camera (RICOH, Caplio R1v, 5.0M PIXELS 4.8X WIDE ZOOM).

### 8 (b) Microscopic observations and microstructure characterization

9 Morphological analyses of the five selected composite samples were performed by Scanning  
10 Electron Microscopy (SEM), with a HITACHI S-4800 microscope. Isolated fine particles  
11 (oriented on carbon Ni grids) of the same selected composite samples were also studied using  
12 a JEOL 3010 Transmission Electron Microscope (TEM) equipped with an energy dispersive  
13 X-ray analyzer (EDS) to image the morphology of the particles and to identify the  
14 precipitated phases.

15 The starting materials (Ca(OH)<sub>2</sub> and selenocystine) and four selected composite samples were  
16 characterized by X-ray powder diffraction using a Kristalloflex 810, SIEMENS  
17 diffractometer in Bragg-Brentano geometry. The XRD patterns were collected using Co  $k\alpha_1$   
18 ( $\lambda_{k\alpha_1}=1.7889 \text{ \AA}$ ) and  $k\alpha_2$  ( $\lambda_{k\alpha_2}=1.7928 \text{ \AA}$ ) radiation in the range  $2\theta = 5 - 80^\circ$  with a step size  
19 of  $0.02^\circ$  and a counting time of 8 seconds per step.

20 The selenocystine powder and three selected composite samples (water-saturated materials:  
21 pasties) were also characterized by XANES and EXAFS spectroscopy. X-ray Absorption  
22 Near-Edge (XANES) and Extended X-ray Absorption Fine-Structure (EXAFS) spectra were  
23 collected at the Rossendorf Beamline at ESRF (Grenoble, France) using a 13-element high-  
24 purity germanium detector (Canberra) together with a digital signal processing unit (XIA) for  
25 fluorescence detection. For energy calibration, a gold foil (K-edge at 11919 eV) was chosen



1 because of its greater inertness and hence reliability in comparison to Se. With this approach,  
2 we determined an edge energy of 12656 eV for trigonal Se, instead of the tabulated value of  
3 12658 eV for zerovalent Se. Dead time correction of the fluorescence signal, energy  
4 calibration and the averaging of single scans, as well as linear combination fits were  
5 performed with the software package SixPack. Shell fitting was done in WinXAS.

6

### 7 *2.3. Physicochemical characterization of aqueous solutions*

#### 8 (a) Total element-concentration and pH

9 10 ml for all sampled suspensions were filtered through a 0.22 $\mu$ m pore-size filter and the  
10 obtained aqueous solutions were immediately acidified with a nitric acid solution and stored  
11 at 4°C for further measurement of [Ca] and [Se] by Inductively Coupled Plasma Atomic  
12 Emission Spectrometry (ICP Perkin Elmer Optima 3300 DV). The pH was also systematically  
13 measured at 25°C by using a MA235 pH/ion analyser in filtered solutions without  
14 acidification.

15

#### 16 (b) Selenium speciation

17 10 ml for twelve sampled suspensions corresponding to two selected experiments were  
18 filtered through a 0.22 $\mu$ m pore-size filter and the obtained aqueous solutions were  
19 immediately stored at 4°C for further measurement (after one week) of selenocystine  
20 (SeCyst), selenomethionine (SeMet), selenite (Se(IV)) and selenate (Se(VI)) by liquid  
21 chromatography coupled with ICPMS detection (HPLC/ICPMS). The conditions for  
22 determination of SeCyst, SeMet, Se(IV) and Se(VI) species have been previously described  
23 [30]. Briefly, chromatographic separation was carried out using the Agilent 1100 series HPLC  
24 pump, equipped with an autosampler and variable volume sample loop. The analytical column  
25 was a Hamilton PRP-X-100, 10 $\mu$ m particle size, 25 cm length x 4.1 mm internal diameter.

1 The chromatographic separation of the four selenium species was obtained using a 5 mmol l<sup>-1</sup>  
2 ammonium citrate buffer at pH 5.2. Injection volume was fixed at 100 μL. Low percentage of  
3 methanol (2% v/v) was added in the mobile phase to improve sensitivity. The mobile phase  
4 was delivered at 1ml min<sup>-1</sup> isocratically. The HPLC-ICPMS interface consisted simply in a  
5 polyetheretherketone (PEEK) tube. Selenium selective detection was performed with an  
6 Agilent 7500ce ICPMS equipped with collision reaction cell. The instrumental and  
7 acquisition parameters were: rf power (1500 W); carrier gas (1 L/min); reaction cell gas (H<sub>2</sub> at  
8 5.0 mL/min). Integration time was 0.4 s for both *m/z* 77 and 78. Selenium species were  
9 quantified in diluted samples (1/10000) by external calibration with standard solutions of the  
10 respective pure compounds. Quantification was performed with selenium isotope *m/z* 78.

11

### 12 **3. Results and discussion**

13

#### 14 *3.1. Characterization of Se<sup>0</sup>/calcite composite produced under O<sub>2</sub>-poor conditions*

15 Macroscopically, the typical colour of calcite is white, while the typical colours of Se<sup>0</sup> are  
16 grey and red. In the current study, a red composite was produced under O<sub>2</sub>-poor conditions.  
17 The red coloration depended on the selenocystine dose, for example, it was noticed that the  
18 red coloration of composite started to be observable when 50 mg/kg<sub>water</sub> were used and the  
19 colour intensity increased with an increase of selenocystine dose (Figure 2). This coloration  
20 behaviour was reproducible at a constant calcium hydroxide dose (3 g/kg<sub>water</sub> for this study).  
21 The coloration of composite was stable in its mother aqueous solution even after several  
22 weeks of storage at room conditions and without protection to the light.

23 Microscopically, the red composite was mainly characterized by spherical selenium  
24 nanoparticles (< 500 nm) deposited on the calcite matrix. The carbonate matrix was

1 constituted by nano- and micro rhombohedral crystals ( $< 2 \mu\text{m}$ ) and micrometric  
2 agglomerates and/or aggregates ( $< 5 \mu\text{m}$ ) (Figure 3).

3 Finally, the microstructure characterization of the red composite by using x-ray diffraction,  
4 suggests a complete  $\text{Ca(OH)}_2$ -calcite conversion, i.e. that the metastable crystalline phases of  
5  $\text{CaCO}_3$ , such as vaterite and aragonite were not produced during the  $\text{Ca(OH)}_2$  carbonation  
6 process in our experiments. Concerning the selenocystine, this crystalline organic material  
7 was not identified on the x-ray diffraction spectra for red  $\text{Se}^0$ /calcite composite (Figure 4).  
8 This suggests a complete chemical transformation or water dissolution of this starting solid  
9 material in our experiments and justifies the precipitation of red nano-particles of elemental  
10 selenium (observed by SEM and TEM microscopy), but, these results do not give any  
11 information on the selenocystine fragmentation mechanism. **Note that red elemental selenium**  
12 **“spherical Se nanoparticles” was not identified by X-ray powder diffraction due to its poor**  
13 **crystalline property or amorphous property for this selenium form.**

14

### 15 *3.2. Characterization of $\text{Se}^0$ /calcite composite produced under $\text{O}_2$ -rich conditions*

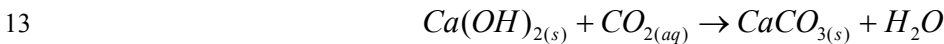
16 For these experiments, it was demonstrated that a grey composite can be produced under  $\text{O}_2$ -  
17 rich conditions. For this case, the grey intensity seems to be slightly dependent on the  
18 selenocystine dose from 50 to 200  $\text{mg/kg}_{\text{water}}$ . The composite coloration was also stable in its  
19 mother aqueous solution even after several weeks of storage at room conditions and without  
20 protection to the light. Microscopic observations showed that the composite was characterized  
21 by rod hexagonal selenium microparticles ( $< 25 \mu\text{m}$ ) dispersed in the calcite matrix (Figure 5).  
22 In addition, the X-ray diffraction measurements support these microscopic observations. It is  
23 well known that the trigonal or hexagonal morphologies are the most stable crystalline phases  
24 for  $\text{Se}^0$ . Here, a small proportion contained in a given composite can be identified by X-ray  
25 diffraction measurements (Figure 6). This figure also show a complete  $\text{Ca(OH)}_2$ -Calcite

1 conversion under O<sub>2</sub>-rich conditions, revealing that the oxygenated conditions in the  
 2 suspension have not significant effect on the carbonation process efficiency. However, the  
 3 available quantity of oxygen in the suspension controls the fragmentation process of the  
 4 selenocystine, leading the precipitation/growth of elemental selenium with two different  
 5 morphologies and different sizes of particles. Consequently, it is demonstrated that the  
 6 fragmentation process of selenocystine under O<sub>2</sub>-poor or O<sub>2</sub>-rich conditions participates to the  
 7 precipitation/growth of calcite with unusual morphologies. This will be qualitatively  
 8 described in the following sub-section.

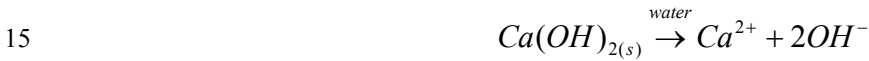
9

### 10 3.3. Precipitation/growth of calcite with unusual morphologies

11 For our experiments, the hydrothermal carbonation of calcium hydroxide described by the  
 12 global well-known reaction,



14 is an exothermic process that concerns simultaneously the dissolution of Ca(OH)<sub>2</sub>,



16 and the dissociation of aqueous CO<sub>2</sub>,



18 These processes produce a fast supersaturation ( $S_I$ ) of the solution with respect to calcite,

$$19 \quad S_I = \frac{(Ca^{2+})(CO_3^{2-})}{K_{sp}} > 1$$

20 where ( $Ca^{2+}$ ) and ( $CO_3^{2-}$ ) are the activities of calcium and carbonate ions in the solution,  
 21 respectively, and  $K_{sp}$  is the thermodynamic solubility product of calcite. Then, the nucleation  
 22 stage (formation of nuclei or critical cluster) takes place in the system,



1 The sampling with time of the suspensions in the reactor allowed the identification of the  
2 nucleation stage, characterized by the formation of an apparent stable emulsion after about  
3 two minutes of reaction time.

4 Finally, the crystal growth occurred spontaneously until the equilibrium calcite and the  
5 solution was reached,



7 For this study, it was demonstrated that the selenocystine fragmentation during heating and  
8 carbonation process had insignificant effect on the  $Ca(OH)_2$ -calcite conversion, its effect on  
9 the calcite precipitation rate was not clear because the kinetic behaviour of ex-situ pH and Ca-  
10 concentration of sampled solutions were very similar for all experiments. However, several  
11 TEM micrographs revealed an unusual agglomeration/aggregation process of rhombohedral  
12 particles, this leading the unusual morphologies for calcite “ex. star-like morphologies” (see  
13 Figure 7). Recent microscopic observations show that the star-like morphologies in the solid  
14 product correspond to a physical aggregation of the crystalline nano-particles of calcite. This  
15 was attested by a simple physical treatment, i.e. by gently ground of composite product in a  
16 mortar in presence of ethanol. After this treatment, the star-like morphologies were not  
17 observed (unpublished data). For this case, the nanoparticles formation can be explained by  
18 the classic theory on the inhibition crystal growth, i.e. the surface poisoning of calcite nuclei  
19 by adsorption/incorporation of selenite ( $SeO_3^{-2}$ ) and other unidentified impurities in-situ  
20 produced during selenocystine fragmentation process (see Table 1 and sub-section 3.4). In  
21 addition, recent studies in our research group shows that the incorporation of selenite ( $SeO_3^{-2}$ )  
22 into calcite retards the  $CO_2$  transfer in the suspension during  $Ca(OH)_2$  carbonation process  
23 (see Fig. A in the Supporting Information).

24

1 On the other hand, It is well known that impurities and additives in the solution can be modify  
2 crystal habits and could induce crystallographic twinning, which has been implicitly assumed  
3 to result from sorption of impurity/additive to the growing crystal surfaces, thus altering the  
4 growth kinetics. Recently, in-situ observations reveal that polyaspartate induces liquid-liquid  
5 phase separation of droplets of a mineral precursor. The droplets deposit on the substrate and  
6 coalesce to form a coating, which then solidifies into calcitic tablets and films. Transition bars  
7 form during the amorphous to crystalline transition, leading to sectorization of calcite tablets,  
8 and the defect textures and crystal morphologies are atypical of solution grown crystals [31-  
9 34].

10

#### 11 *3.4. Selenocystine fragmentation process*

12 The powdered selenocystine is slightly soluble in pure water at atmospheric conditions, but a  
13 small dissolved amount increases the solution pH from 5.8 to about 8.5 due to a high proton  
14 ( $H^+$ ) affinity of the two amine groups. The liquid chromatography coupled to ICPMS  
15 detection has shown that the selenocystine molecule can be conserved during several weeks in  
16 HCl acidic solution (pH=1) and preferentially at high selenocystine concentration (1 g(Se)/L)  
17 [35].

18 This same analytical technique revealed that selenocystine was rapidly fragmented in  
19  $Ca(OH)_2$  alkaline solutions (pH  $\cong$  12.5 measured at 25°C). Here, about 25% of initial atomic  
20 selenium contained in the selenocystine (experiment with 200mg/kg<sub>water</sub>) was oxidized to  
21 Se(IV) under O<sub>2</sub>-poor conditions. Conversely, about 40% of initial atomic selenium contained  
22 in the selenocystine (experiment with 100mg/kg<sub>water</sub>) was mainly oxidized to Se(IV) and a  
23 slight amount oxidized to (VI) under O<sub>2</sub>-rich conditions (see Table 1). This partial oxidation  
24 of selenocystine taken place before the carbonation process; i.e. before the injection of CO<sub>2</sub> in  
25 the reactor ( $t=0$ ). This confirms the instability of selenocystine in alkaline solutions, in fact,

1 the SeCyst instability seems be controlled by the initial dose and the amount of dissolved  
2 oxygen.

3 Note also in Table 1 that before the CO<sub>2</sub> injection in the reactor ( $t=0$ ), the selenocystine was  
4 slightly detected in the solution, but the kinetic data revealed a selenocystine  
5 desorption/liberation process from Ca(OH)<sub>2</sub> particles during carbonation process ( $t\neq 0$ ), this  
6 effect being preferentially noticed under O<sub>2</sub>-poor conditions. This suggests that a significant  
7 proportion of the initial SeCyst was adsorbed onto the Ca(OH)<sub>2</sub> particles. Consequently, at  
8 higher adsorbed quantity of SeCyst, i.e. under O<sub>2</sub>-poor conditions, the precipitation/growth of  
9 spherical nanoparticles of red elemental selenium was favoured during the carbonation  
10 process. Conversely, at lower adsorbed quantity of SeCyst, i.e. under O-rich conditions, the  
11 precipitation/growth of hexagonal microparticles of gray elemental selenium was favoured  
12 during carbonation process.

13 The selenite-oxyanion produced during heating of Ca(OH)<sub>2</sub> suspension follows a complex  
14 path during carbonation process. Firstly, its solution concentration was drastically decreased  
15 by adsorption/incorporation on/in calcite matrix, leading the unusual morphologies for calcite  
16 “ex. star-like morphologies” (Figure 7). And secondly, a slight concentration increase was  
17 observed caused by a dissolution process of calcite fine particles due to a high molar excess of  
18 CO<sub>2</sub> in the system.

19 The adsorption and/or incorporation of selenite (SeO<sub>3</sub><sup>-2</sup>) on/in the calcite were supported by  
20 XANES and EXAFS spectrometry. This powerful technique allowed also the identification  
21 and quantification of different selenium forms co-existed with calcite for three selected solid  
22 samples (labelled calcite 2, calcite 3 and calcite 5 in figures 8 and 9).

23 The Se K-edge XANES spectra of the three calcite samples are dominated by a white line at  
24 12,656.5 eV, indicative of elemental Se (Figure 8.) [36-37]. Since the white line peak position  
25 of selenocystine is about 2 eV above that of elemental Se, we can discard that substantial

1 amounts of selenocystine is present in the samples. Samples 3 and 5 have an additional strong  
2 oscillation at 12,662 eV, which coincides with the white line of Se(IV), indicating that these  
3 samples contain tetravalent Se in addition to elemental Se.

4 The corresponding Se K-edge EXAFS are shown in Figure 9. The Fourier transform peaks at  
5 about 2.1 Å (uncorrected for phase shift) in the spectra of elemental Se and of selenocystine  
6 are due to Se-Se backscattering within the coordination sphere. This is also the strongest peak  
7 in the Fourier transform spectra of the three calcite samples. Red and gray elemental Se are  
8 discernable by the intensity of the 1st and 2<sup>nd</sup> shells, the ones for gray Se being much stronger  
9 due to the higher structural order. The spectrum of sample 5 is very similar to that of gray Se,  
10 while samples 2 and 3 are closer to red Se. The Se-O backscattering peak of the Se(IV)  
11 reference, Na<sub>2</sub>SeO<sub>3</sub>, occurs at a smaller distance of 1.4 Å. All three sample spectra show a  
12 contribution from this shell, although much lower in intensity than the pure Se(IV)  
13 compound. We can therefore conclude that all samples contain a small amount of Se(IV)  
14 adsorbed/incorporated onto/into calcite in addition to Se(0). This is in agreement with  
15 XANES results.

16 To further support this tentative phase identification and to derive quantitative information,  
17 we performed linear combination fits of the k<sup>3</sup>-weighted EXAFS spectra (Table 2). In  
18 confirmation of the visual interpretation of EXAFS spectra, sample calcite 5 contains a large  
19 amount of gray Se, while the other two samples are dominated by red Se. Note that satisfying  
20 fits were achieved only, when a reference spectrum of the aqueous selenite was added for  
21 samples calcite 2 and calcite 3, and the reference spectrum of a Se(IV) solid phase was added  
22 for sample calcite 5. The relative amount of Se(IV) corresponds to the relative height of the  
23 Se-O Fourier peak (Figure 9).

24 The sampling with time in the reactor and the use of multi-technique approach give relevant  
25 information on the selenocystine fragmentation process for our experiments, but, with this



1 information is still difficult to propose a clear chemical reaction mechanism. Note for  
2 example, that three transient selenium species were not identified and quantified by using  
3 HPLC/ICPMS measurements (Table 1) because only four selenium references were initially  
4 considered for this study.

5

#### 6 **4. Conclusion**

7

8 In this study, the main purpose was to synthesize a  $\text{Se}^0$ /calcite composite. The synthesis was  
9 successfully performed by using the hydrothermal carbonation of calcium hydroxide under  
10 high  $\text{CO}_2$ -Ar pressure and high temperature coupled with a complex selenocystine  
11 fragmentation process under  $\text{O}_2$ -poor and  $\text{O}_2$ -rich conditions. In conclusion, under  $\text{O}_2$ -poor  
12 conditions (i.e. with purge stage), the composite was mainly characterized by spherical  
13 selenium nanoparticles ( $<500\text{nm}$ ) deposited on the calcite matrix. The carbonate matrix was  
14 constituted by nano- and micro rhombohedral crystals ( $<2\mu\text{m}$ ) and micrometric agglomerates  
15 and/or aggregates ( $<5\mu\text{m}$ ). For this case, the spherical Se nanoparticles give a stable red  
16 coloration to the composite. In contrast, under  $\text{O}_2$ -rich conditions (i.e. without purge stage),  
17 the composite was characterized by hexagonal selenium microparticles ( $<25\mu\text{m}$ ) dispersed in  
18 the calcite matrix. For this case, a gray coloration of composite was observed. It was also  
19 observed that the gas purge in the system and the selenocystine dose ( $\text{mg}/\text{kg}_{\text{water}}$ ) play a  
20 crucial role on the selenocystine fragmentation mechanism during  $\text{Ca}(\text{OH})_2$  suspension  
21 heating (at  $90^\circ\text{C}$ ) and carbonation stages, this leading the precipitation/growth of elemental  
22 selenium with different morphologies and particle sizes. Consequently, it was noticed that the  
23 selenocystine fragmentation participates to the precipitation/growth of calcite with unusual  
24 morphologies “ex. star-like morphologies”.

1 Finally, the results presented here demonstrate that Se<sup>0</sup>/calcite composite, with spherical or  
2 hexagonal morphologies for elemental selenium can be produced, this composite possibly  
3 with a high potential for medical (ex. dietary supplement) or industrial (ex. pigments)  
4 applications.

5

6

7

8

9

10

11

12

13

14

15

16

17

18

19

20

21

22

23

24

25

1 **Acknowledgements**

2

3 The authors are grateful to the National Research Agency, ANR (GeoCarbone-  
4 CARBONATATION project), France, for providing a financial support for this work. J.  
5 Ganbaja, A. Kohler, D. Tisserand and N. Geoffroy are thanked for their technical help and  
6 assistance.

7

8

9

10

11

12

13

14

15

16

17

18

19

20

21

22

23

24

25

## References

- [1] J. M. Song, J. H. Zhu, S. H. Yu, *J. Phys. Chem. B.* 110 (2006) 23790.
- [2] Y. Ding, Q. Li, Y. Jia, L. Chen, J. Xing, Y. Qian, *J. Crystal Growth* 241 (2002) 489.
- [3] Y. Bai, Y. Wang, Y. Zhou, W. Li, W. Zheng, *Materials Letters* (2007) doi:10.1016/j.matlet.2007.11.098.
- [4] E. Kapolna, M. Shah, J. A. Caruso, P. Fodor, *Food Chemistry* 101 (2007) 1398.
- [5] A. Tarze, M. Dauplais, I. Grigoras, M. Lazard, N. T. Ha-Duong, F. Barbier, S. Blanquet, P. Plateau, *J. Biol. Chem.* 282/12 (2007) 8759.
- [6] R. Caputo, S. Capone, M. Della Greca, L. Longobardo, G. Pinto, *Tetrahedron Letters* 48 (2007) 1425.
- [7] D. Peng, J. Zhang, Q. Liu, E. Will Taylor, *J. Inorg. Biochem.* 101 (2007) 1457.
- [8] J. E. Spallholz, D. J. Hoffman, *Aquatic Toxicology* 57 (2002) 27.
- [9] M. S. Stewart, J. E. Spallholz, K. H. Neldner, B. C. Pence, *Free Radic. Biol. Med* 26 (1999) 42.
- [10] M. Ochsenkuhn-Petropoulou, F. Tsopelas, *Anal. Chim. Acta* 467 (2002) 167.
- [11] K. H. Goh, T. T. Lim, *Chemosphere* 55, (2004) 849.
- [12] C. Munier-Lamy, S. Deneux-Mustin, C. Mustin, D. Merlet, J. Berthelin, C. Leyval, *J. Environ. Radioactivity* (2007) doi :10.1016/j.jenvrad.2007.04.001
- [13] M. Simonoff, C. Sergeant, S. poulain, M. S. Pravikoff, *Comptes Rendus Chimie* (2007) doi :10.1016/J.crci.2007.02.010
- [14] Y. S. Han, G. Hadiko, M. Fuji, M. Takahashi, *J. Crystal Growth* 276 (2005) 541.
- [15] L. Moore, J. D. Hopwood, R. J. Davey, *J. Crystal Growth* 261 (2004) 93.
- [16] K. J. Westin, A. C. Rasmuson, *J. Colloids Interface Sci.* 282 (2005) 370.
- [17] H. Tsuno, H. Kagi, T. Akagi, *Bull. Chem. Soc. Jpn.* 74 (2001) 479.

- 1 [18] Y. Fujita, G. D. Redden, J. Ingram, M. M. Cortez, G. Ferris, R. W. Smith, *Geochem.*  
2 *Cosmochem. A.* 68 (2004) 3261.
- 3 [19] S. J. Freij, A. Godelitsas, A. Putnis, *J. Crystal Growth* 273 (2005) 535.
- 4 [20] L. A. Gower, D. A. Tirrell, *J. Crystal Growth* 191 (1998) 153.
- 5 [21] R. G. Jonasson, K. Rispler, B. Wiwchar, W. D. Gunter, *Chem. Geol.* 132 (1996) 215.
- 6 [22] A. Chrissanthopoulos, N. P. Tzanetos, A. K. Andreopoulou, J. Kallitsis, E. Dalas, *J.*  
7 *Crystal Growth* 280 (2005) 594.
- 8 [23] M. Menadakis, G. Maroulis, P. G. Koutsoukos, *Computational Materials Science* 38  
9 (2007) 522.
- 10 [24] E. Dousi, J. Kallitsis, A. Chrissanthopoulos, A. H. Mangood, E. Dalas, *J. Crystal*  
11 *Growth* 253 (2003) 496.
- 12 [25] L. Pastero, E. Costa, B. Alessandria, M. Rubbo, D. Aquilano, *J. Crystal Growth* 247  
13 (2003) 472.
- 14 [26] Y. J. Lee, R. Reeder, *Geochem. Cosmochem. A.* 70 (2006) 2253.
- 15 [27] M. Temmam, J. Paquette, H. Vali, *Geochem. Cosmochem. A.* 64 (2000) 2417.
- 16 [28] E. Dalas, A. Chalias, D. Gatos, K. Barlos, *J. Colloids Interface Sci.* 300 (2006) 536.
- 17 [29] G. Montes-Hernandez, F. Renard, N. Geoffroy, L. Charlet, J. Pironon, *J. Crystal Growth*  
18 308 (2007) 228.
- 19 [30] J. Darrouzès, M. Bueno, S. Simon, F. Pannier, M. Potin-Gautier, *Talanta* (2007)  
20 doi:10.1016/j.talanta.2007.11.020
- 21 [31] L. B. Gower, D. J. Odom, *J. Crystal Growth* 210 (2000) 719.
- 22 [32] X. Cheng, P. L. Varona, M. J. Olszta, L. B. Gower, *J. Crystal Growth* 307 (2007) 395.
- 23 [33] X. Cheng, L. B. Gower, *Biotechnol. Prog.* 22 (2006) 141.
- 24 [34] L. Dai, A. P. Douglas, L. B. Gower, *J. Non-Crystalline Solids* (2007) doi:  
25 10.1016/j.jnoncrysol.2007.10.022

1 [35] M. Bueno, (2007) *personal interview*

2 [36] A. C. Scheinost, L. Charlet, Environ. Sci. Technol. (2007) in press.

3 [37] L. Charlet, A. C. Scheinost, C. Tournassat, J. M. Greneche, A. Gehin, A. Fernandez-  
4 Martinez, S. Coudert, D. Tisserand, J. Brendle, Geochim. Cosmochim. Acta 71 (2007) 5731.

5

6

7

8

9

10

11

12

13

14

15

16

17

18

19

20

21

22

23

24

25

1 Table 1. The HPLC/ICPMS measurements of twelve solutions samples of two selected  
 2 hydrothermal carbonation-selenocystine fragmentation experiments. Concentrations given in  
 3 mg (Se) l<sup>-1</sup>  
 4

<i>t</i> min	SeCyst	SeIV	SeVI	<i>t<sub>R</sub></i> 2.80 min	<i>t<sub>R</sub></i> 5.91 min	<i>t<sub>R</sub></i> 7.03 min	pH <sub>25°C</sub>
Under O <sub>2</sub> -poor conditions and 200 mg/kg <sub>water</sub> of SeCyst dose							
0	0.86 ± 0.08	24 ± 1	nd	ni		ni	12.60
2	nd	9.1 ± 0.7	nq		ni		12.43
6	8.9 ± 0.4	0.37 ± 0.01	nq		ni		7.44
10	9.3 ± 0.1	0.95 ± 0.02	nd		ni		7.30
30	4.0 ± 0.2	1.7 ± 0.2	nq		ni		7.34
60	nd	2.5 ± 0.1	nd				7.10
Under O <sub>2</sub> -rich conditions and 100 mg/kg <sub>water</sub> of SeCyst dose							
0	nd	17 ± 1	0.21 ± 0.02	ni	ni		12.63
2	nd	4.7 ± 0.2	0.27 ± 0.01		ni		12.58
6	0.68 ± 0.05	1.5 ± 0.1	0.22 ± 0.2				8.03
10	0.65 ± 0.05	4.0 ± 0.3	0.27 ± 0.02				7.30
30	0.15 ± 0.03	5.6 ± 0.2	0.25 ± 0.02				7.28
60	nd	5.7 ± 0.3	0.24 ± 0.02				7.15

5 *t*: reaction time concerning the experiment (*t*=0 “before CO<sub>2</sub> injection in the reactor”); SeCyst: seleno-L-cystine;  
 6 SeIV: selenite (SeO<sub>3</sub><sup>-2</sup>); SeVI: selenate (SeO<sub>4</sub><sup>-2</sup>); *t<sub>R</sub>*: retention time in the HPLC/ICPMS measurements; pH<sub>25°C</sub>:  
 7 pH measured at 25°C; nd: not detected; nq: not quantifiable; ni: not identifiable.  
 8  
 9

10

11

12

13

14

15

16

17

1            Table 2. Linear combination fit of  $k^3$ -weighted EXAFS spectra

Sample	Se grey	Se red	Se(IV)	Sum
Calcite 2	0.02	0.87	0.12	1.01
Calcite 3	0.15	0.50	0.28	0.93
Calcite 5	0.74	0.07	0.23	1.04

2 Calcite 2: experiment under O<sub>2</sub>-poor conditions, 100 mg/kg<sub>water</sub> of selenocystine, 1 hour of reaction. Calcite 3:  
 3 experiment under O<sub>2</sub>-poor conditions, 50 mg/kg<sub>water</sub> of selenocystine, 1 hour of reaction. Calcite 5: experiment  
 4 under O<sub>2</sub>-rich conditions, 100 mg/kg<sub>water</sub> of selenocystine, 1 hour of reaction. Se(IV) correspond to Se(IV)<sub>aquo</sub>  
 5 and Na<sub>2</sub>SeO<sub>3</sub> references in Charlet et al., 2007 [37].  
 6

7

8

9

10

11

12

13

14

15

16

17

18

19

20

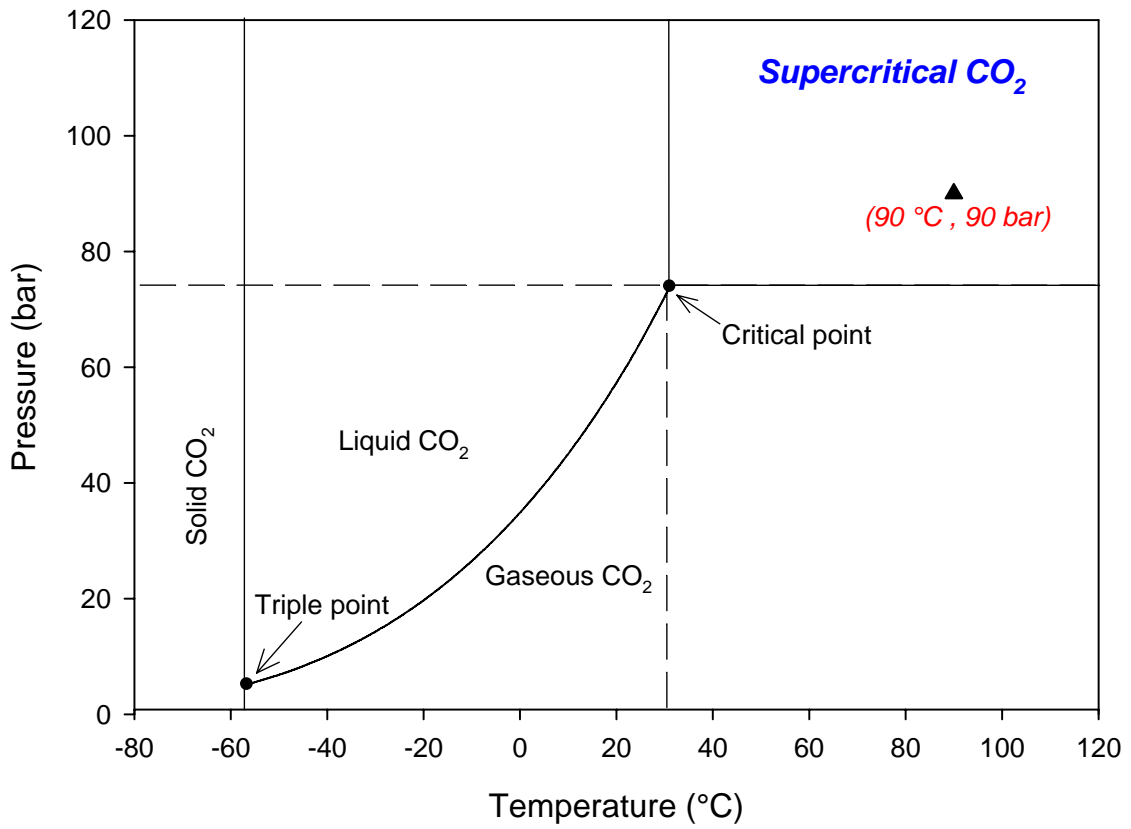
21

22

23

24

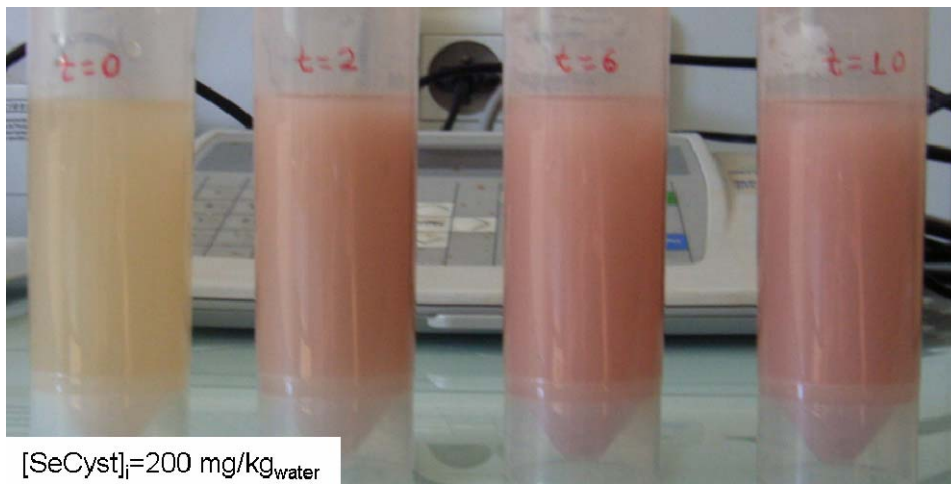
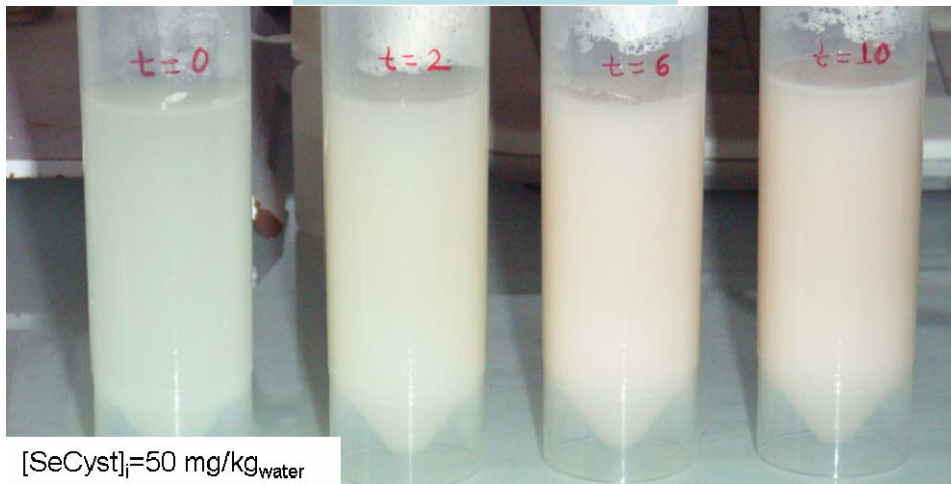




1  
2  
3  
4  
5  
6  
7  
8  
9  
10  
11  
12  
13

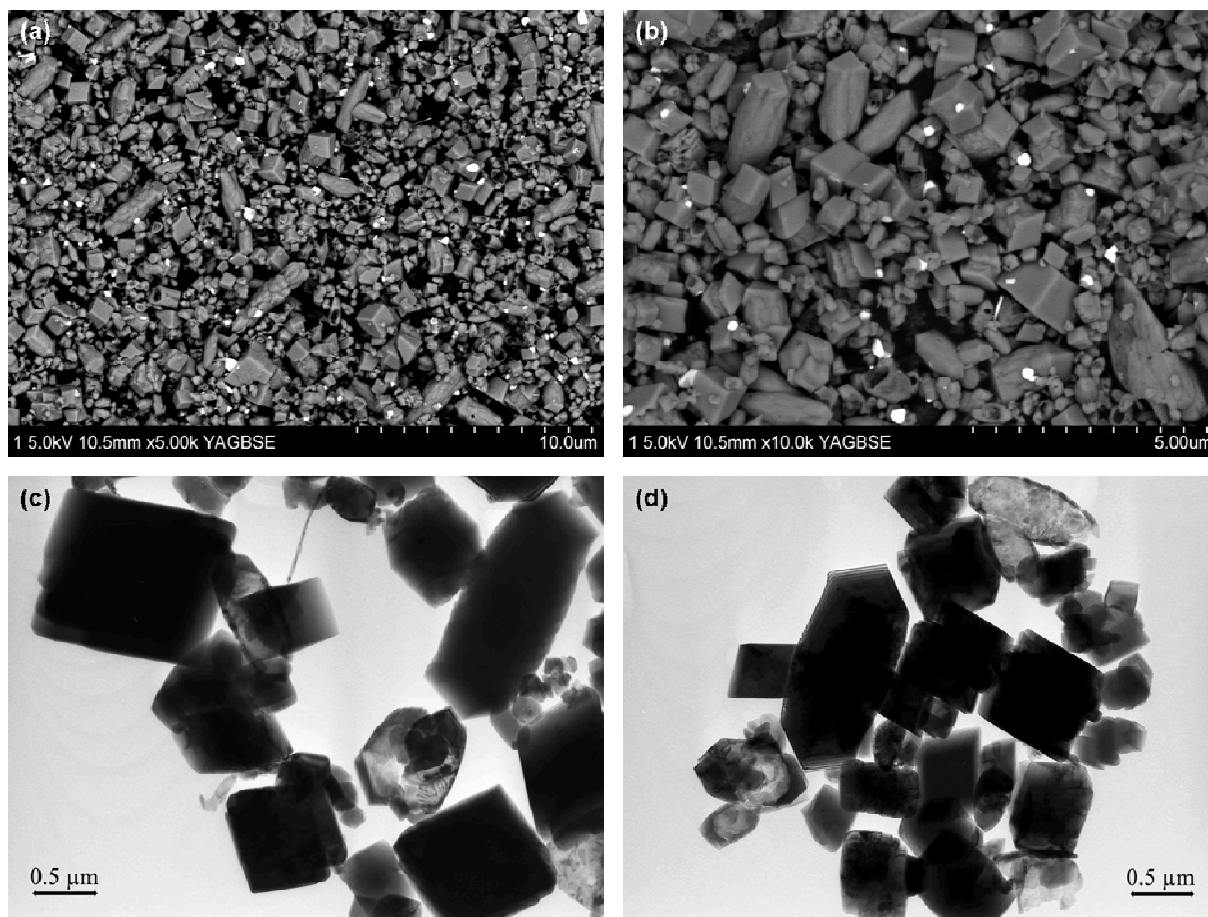
Figure 1. Experimental P-T conditions represented on a pressure-temperature phase diagram for CO<sub>2</sub>

Under O<sub>2</sub>-poor conditions



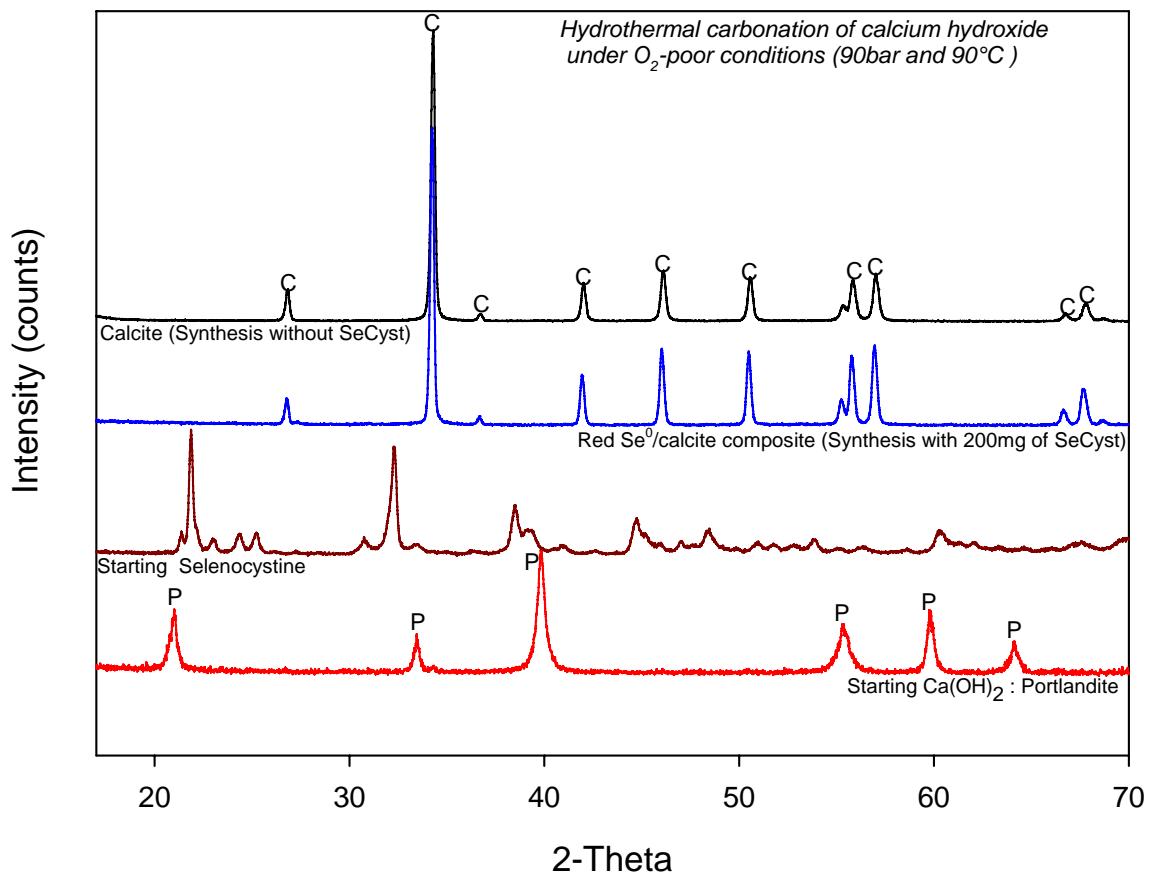
1  
2  
3  
4  
5  
6  
7  
8  
9  
10  
11

Figure 2. Coloration change of Se<sup>0</sup>/calcite composite at different selenocystine doses and under O<sub>2</sub>-poor conditions. Note the Se<sup>0</sup>/calcite composite was manually dispersed to take these photographs.



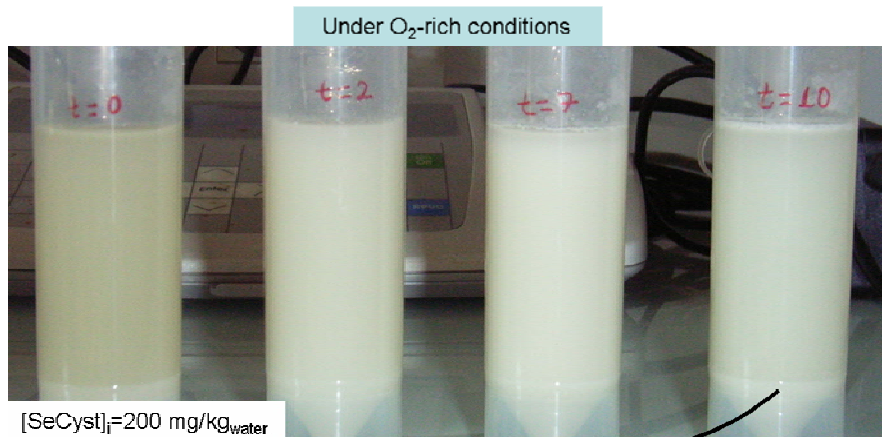
1  
2  
3  
4  
5  
6  
7  
8  
9  
10  
11  
12

Figure 3. Red  $\text{Se}^0$ /calcite composite synthesized by hydrothermal carbonation of calcium hydroxide coupled with a complex selenocystine fragmentation under  $\text{O}_2$ -poor conditions. (a) and (b) Backscattering SEM observations “without metal coating”; (c) and (d) TEM micrographs.



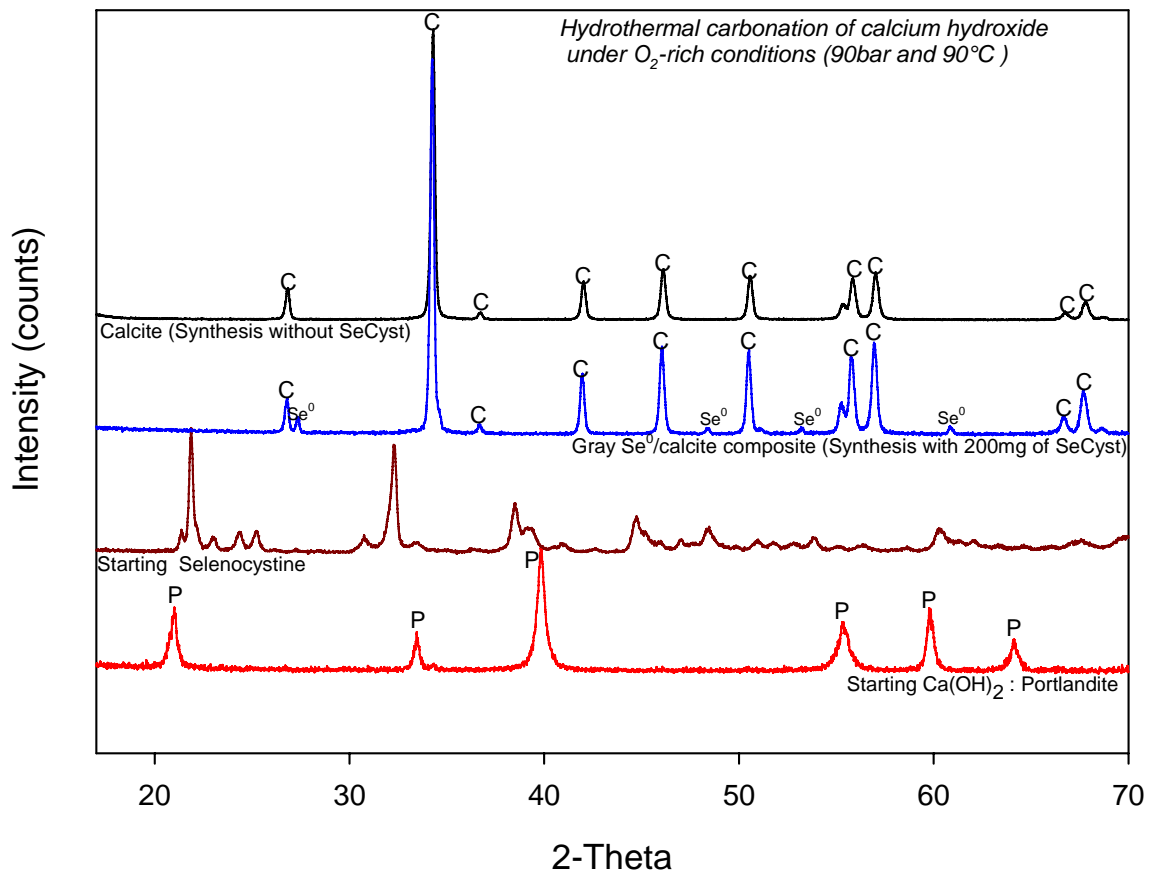
1  
2  
3  
4  
5  
6  
7  
8  
9

10 Figure 4. XRD measurements of starting solid materials (calcium hydroxide and  
 11 selenocystine) and solid products (pure calcite and red Se<sup>0</sup>/calcite composite).  
 12 Hydrothermal carbonation of calcium hydroxide under O<sub>2</sub>-poor conditions (P=200 bar;  
 13 T=90 °C; Ca(OH)<sub>2</sub> dose=3 g/kg<sub>water</sub>; Selenocystine dose=200 mg/kg<sub>water</sub>; 1 hour of reaction  
 14 time). P: Portlandite, C: Calcite.



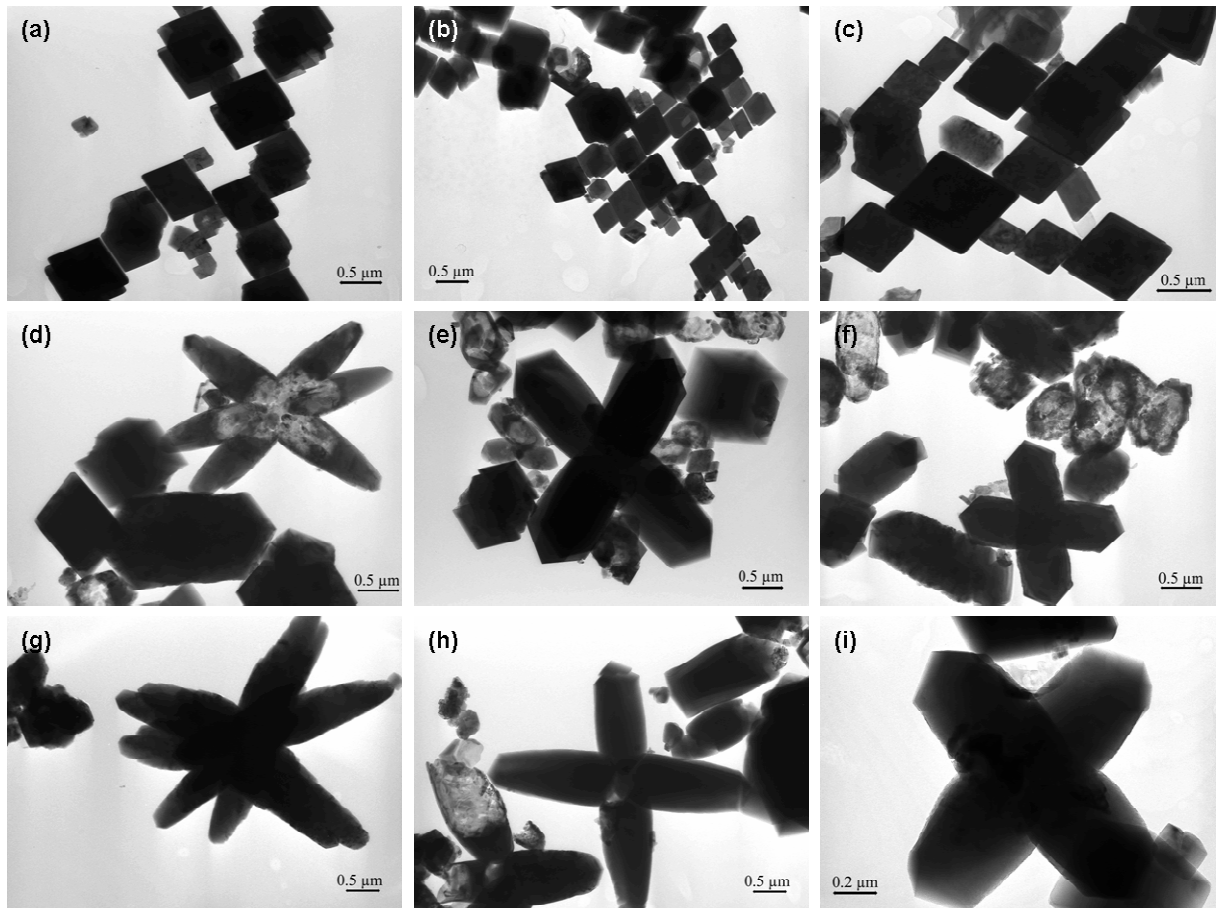
1  
2  
3  
4  
5  
6  
7  
8  
9  
10  
11  
12  
13

Figure 5. Gray Se<sup>0</sup>/calcite composite synthesized by hydrothermal carbonation of calcium hydroxide coupled with a complex selenocystine fragmentation under O<sub>2</sub>-rich conditions. (a) and (b) Backscattering SEM observations “without metal coating”.



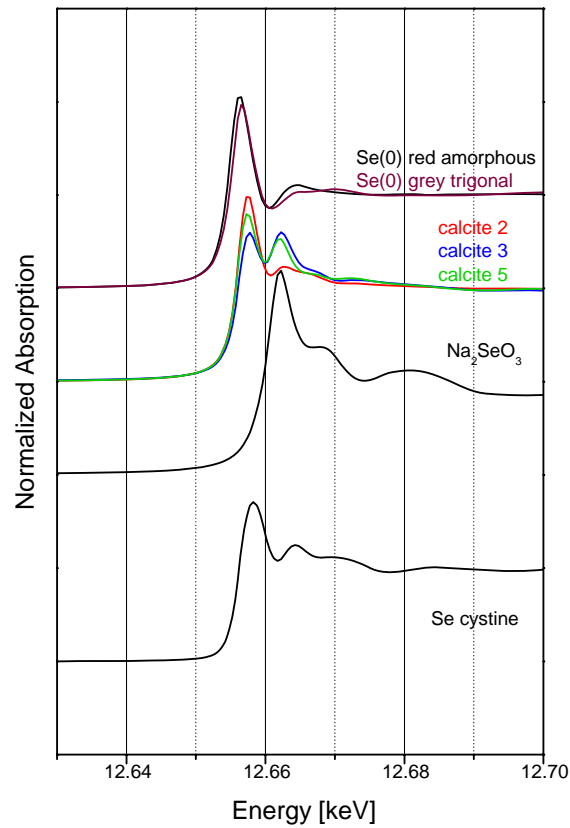
1  
2  
3  
4  
5  
6  
7  
8  
9  
10  
11  
12  
13  
14

Figure 6. XRD measurements of starting solid materials (calcium hydroxide and selenocystine) and solid products (pure calcite and gray Se<sup>0</sup>/calcite composite). Hydrothermal carbonation of calcium hydroxide under O<sub>2</sub>-rich conditions (P=200 bar; T=90 °C; Ca(OH)<sub>2</sub> dose=3 g/kg<sub>water</sub>; selenocystine dose=200 mg/kg<sub>water</sub>; 1 hour of reaction time). P: portlandite, C: calcite.



1  
2  
3  
4  
5  
6  
7  
8  
9  
10  
11  
12  
13  
14

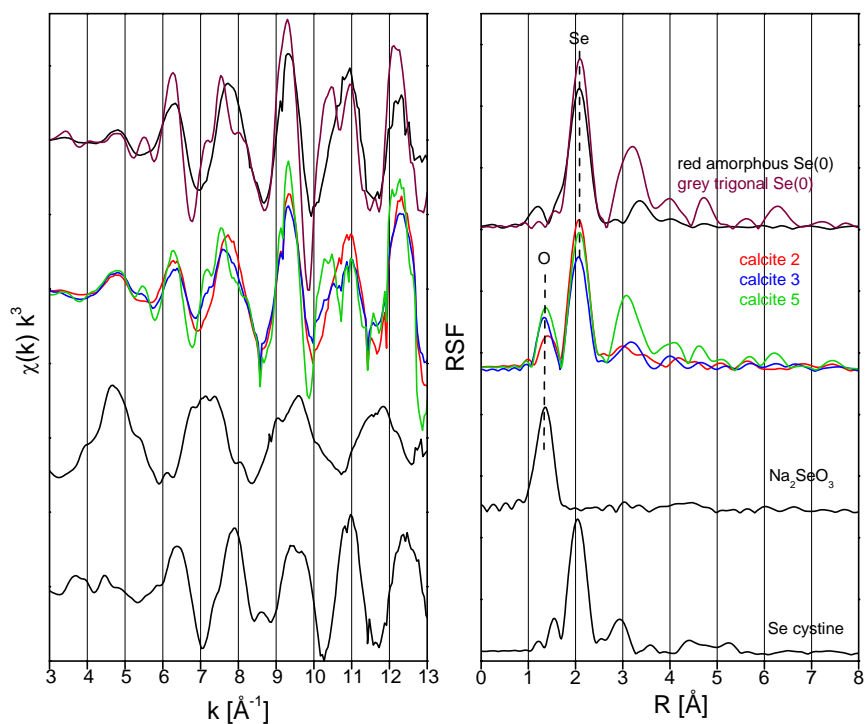
Figure 7. (a), (b) and (c) Rhombohedral nano- and micro-particles of calcite; hydrothermal carbonation process without initial selenocystine dose. (d), (e), (f), (g), (h) and (i) Morphology for calcite “ex. star-like morphologies”; hydrothermal carbonation process with initial selenocystine dose (200 mg/kg<sub>water</sub>)



1  
2  
3  
4  
5  
6  
7  
8  
9  
10  
11  
12  
13  
14

Figure 8. Se K-edge XANES of three calcite samples in comparison to select references. Calcite 2: experiment under O<sub>2</sub>-poor conditions, 100 mg/kg<sub>water</sub> of selenocytine, 1 hour of reaction. Calcite 3: experiment under O<sub>2</sub>-poor conditions, 50 mg/kg<sub>water</sub> of selenocytine, 1 hour of reaction. Calcite 5: experiment under O<sub>2</sub>-rich conditions, 100 mg/kg<sub>water</sub> of selenocytine, 1 hour of reaction. Se cystine correspond to the selenocystine reference.





1  
2  
3  
4  
5  
6  
7  
8  
9  
10

11 Figure 9. Se K-edge EXAFS spectra (left) and corresponding Fourier transforms (right) of the  
 12 three calcite samples and select references. Calcite 2: experiment under O<sub>2</sub>-poor conditions,  
 13 100 mg/kg<sub>water</sub> of selenocystine, 1 hour of reaction. Calcite 3: experiment under O<sub>2</sub>-poor  
 14 conditions, 50 mg/kg<sub>water</sub> of selenocystine, 1 hour of reaction. Calcite 5: experiment under O<sub>2</sub>-  
 15 rich conditions, 100 mg/kg<sub>water</sub> of selenocystine, 1 hour of reaction. Se cystine correspond to  
 16 the selenocystine reference.